

GW quasiparticle band structures of stibnite, antimonelite, bismuthinite, and guanajuatite

Marina R. Filip, Christopher E. Patrick, and Feliciano Giustino

Department of Materials, University of Oxford, Parks Road, Oxford OX1 3PH, United Kingdom

We present first-principles calculations of the quasiparticle band structures of four isostructural semiconducting metal chalcogenides A_2B_3 (with $A = \text{Sb, Bi}$ and $B = \text{S, Se}$) of the stibnite family within the G_0W_0 approach. We perform extensive convergence tests and identify a sensitivity of the quasiparticle corrections to the structural parameters and to the semicore d electrons. Our calculations indicate that all four chalcogenides exhibit direct band gaps, if we exclude some indirect transitions marginally below the direct gap. Our converged quasiparticle band gaps are 1.6 eV (Sb_2S_3), 1.3 eV (Sb_2Se_3), 1.7 eV (Bi_2S_3) and 1.2 eV (Bi_2Se_3). By comparing our calculated gaps with the ideal Shockley-Queisser value we find that all four chalcogenides are promising as light sensitizers for nanostructured photovoltaics.

PACS numbers: 71.20.-b 74.70.Xa 78.20.-e 78.56.-a

I. INTRODUCTION

The development of sustainable energy solutions based on scalable processes and non-toxic materials constitutes a key priority in the current scientific research agenda, and in this area nanostructured energy-harvesting solar and thermoelectric devices are playing a lead role. Recently there has been a surge of interest in devices using semiconducting metal chalcogenides of the stibnite family. For example recent studies have demonstrated the potential of these semiconductors both in photovoltaics applications,¹⁻⁴ and in thermoelectric generators.⁵

In the area of nanostructured photovoltaics semiconducting metal chalcogenides have successfully been used to replace the inorganic dye in dye-sensitized solar cells,⁶ leading to the development of solid-state semiconductor-sensitized solar cells.^{1,7} In these devices thin layers or nanoparticles of the semiconducting chalcogenides act as light absorbers, and upon photoexcitation they transfer an electron to the acceptor (typically TiO_2) and a hole to the hole-transporter (for example a conducting polymer). The record efficiency within this class of devices is 5.1% and was obtained using stibnite (Sb_2S_3) as semiconductor sensitizer.¹

A recent atomistic computational study of photovoltaic interfaces for semiconductor-sensitized solar cells pointed out that, in addition to stibnite, the other members of the stibnite mineral family, namely antimonelite (Sb_2Se_3), bismuthinite (Bi_2S_3), and guanajuatite (Bi_2Se_3), exhibit optical properties similar to stibnite and should be considered as potential candidates for novel semiconductor sensitizers.⁸ Using density-functional calculations and empirical scissor corrections of the band gaps, in Ref.8 it was found that stibnite and antimonelite should form type-II heterojunctions with TiO_2 , while bismuthinite should form a type-I heterojunction and hence would not be able to transfer electrons to TiO_2 . These theoretical predictions have recently been confirmed by the experimental investigations of Refs.4,9, thereby providing a motivation for further studies and for the more sophisti-

cated analysis presented in this work.

The four minerals of the stibnite family crystallize in an orthorhombic structure consisting of parallel one-dimensional $(A_4B_6)_n$ ribbons, with $A = \text{Sb, Bi}$ and $B = \text{S, Se}$. A ball-and-stick model of this structure is shown in Fig. 1. Besides its natural occurrence in mineral form, stibnite can be synthesised using a variety of low-cost fabrication techniques.¹⁰⁻¹⁸ Using these techniques it is possible to obtain a good degree of crystallinity,^{19,20} to control dimensionality,^{5,16,21} and to tune the optical properties.^{16,22-24} Semiconductors of the stibnite family have also been synthesized in various nanostructured forms. For example Refs. 5,14,15 and Refs. 5,24 reported nanowires and nanotubes, respectively, of stibnite, antimonelite and bismuthinite. Nanowires of stibnite were found to exhibit enhanced ferroelectric and piezoelec-

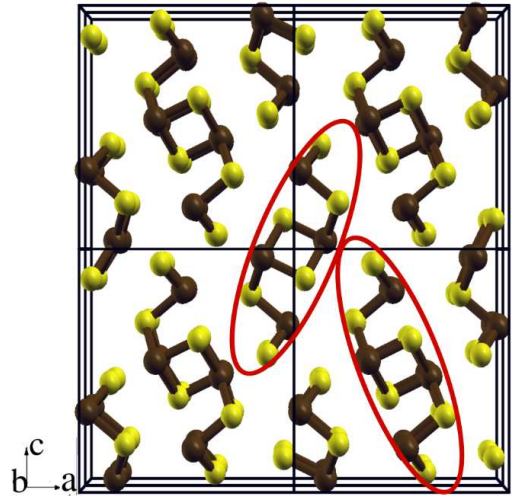


FIG. 1: Ball-and-stick model of A_2B_3 semiconducting metal chalcogenides of the stibnite family, with A standing for Sb or Bi (brown), and B for S or Se (yellow). The two inequivalent $(A_4B_6)_n$ ribbons in the unit cell are highlighted in red, and the perspective view is along the direction of the ribbons.

tric properties as compared to their bulk counterpart.²⁵ Nanowires and nanotubes of antimonelite were found to exhibit conductivities much higher than their bulk counterpart,⁵ and are being considered for thermoelectric applications. In the case of bismuthinite, Ref. 14 reported nanowires with diameters as small as 1.6 nm, corresponding to a transverse size of only two ribbons. The rhombohedral phase of Bi_2Se_3 has been investigated extensively since this compound is a prototypical topological insulator.²⁶ However to the best of our knowledge little is known about orthorhombic Bi_2Se_3 , i.e. guanajuatite, which is stable only at high temperature and pressure.^{27,28}

The band gaps of stibnite, antimonelite and bismuthinite have been measured extensively via optical absorption experiments. The band gap of stibnite ranges between 1.42-1.78 eV.^{29,30} For antimonelite Ref. 31 reported a direct gap of 1.55 eV, while Ref. 32 gave an indirect gap between 1-1.2 eV. The measured band gap of bismuthinite is 1.38-1.58 eV.³³⁻³⁵ The spread in the measured gaps can be attributed to the different preparation conditions used, yielding different degrees of polycrystallinity and even amorphous samples in some cases, and also different stoichiometries. In addition all these compounds exhibit closely lying direct and indirect transitions (cf. Fig. 3 below), thereby complicating the assignment of the nature of the optical gap.

All four minerals of the stibnite family have been investigated in detail using density-functional theory (DFT) calculations. The electronic properties of these compounds have been studied in Refs. 8,36-42, and the elastic and optical properties have been calculated in Ref. 39.

A comparison of the theoretical studies published so far shows some inconsistencies in the calculated band gaps, for example the values reported for stibnite are in the range 1.18-1.55 eV.^{8,36,39,43} As expected all the calculated DFT gaps underestimate the measured band gaps. To the best of our knowledge only one work⁴³ reported a calculation of the quasiparticle band gap of stibnite and antimonelite within the GW approximation.⁴⁴

Within this context there exists a need for detailed and reproducible calculations of the electronic structure of stibnite and related compounds based on state-of-the-art quasiparticle techniques. In line with this need the goal of the present work is to report a systematic and reproducible study of the quasiparticle band structures of all four A_2B_3 semiconducting metal chalcogenides of the stibnite family. An emphasis is placed on convergence tests and on the sensitivity of the quasiparticle corrections to the structural parameters and the inclusion of semicore d states in the calculations.

Our calculated G_0W_0 band gaps are 1.6 eV (Sb_2S_3), 1.3 eV (Sb_2Se_3), 1.7 eV (Bi_2S_3) and 1.2 eV (Bi_2Se_3). These values differ from the corresponding DFT gaps by up to 0.5 eV, and are close to the measured optical gaps. By inspection of the band structures we infer that all four compounds have direct band gaps, although in most cases an indirect transition just below the direct gap (within

0.1 eV) is also possible. The inclusion of semicore electrons in the calculations is found to modify the band gaps by 0.1-0.2 eV. In addition we find that the gaps are rather sensitive to the lattice parameters, as they change by up to 0.3 eV when the lattice parameters are taken from experiment or fully optimized within DFT.

The manuscript is organized as follows. In Sec. II we describe the computational methodology and the convergence tests for the GW calculations. In Sec. III we present our main results, including quasiparticle band structures and band gaps. In Sec. IV we discuss our findings in relation to the photovoltaics applications of the materials considered in this work. In Sec. V we summarize our results and present our conclusions.

II. METHODOLOGY

A. DFT calculations

All DFT calculations are performed using the **Quantum Espresso** package.⁴⁵ The calculations are based on the local density approximation (LDA) to DFT.^{46,47}

Only valence electrons are explicitly described, and the core-valence interaction is taken into account by means of Troullier-Martins pseudopotentials⁴⁸ generated using the **fhi98** code.⁴⁹ In the cases of S (Se) the $3s^23p^4$ ($4s^24p^4$) electrons are included in the valence as usual. For Sb and Bi we generate two sets of pseudopotentials, one set with five electrons in the valence, i.e. $5s^25p^3$ and $6s^26p^3$ respectively, and one set with additional semicore $4d^{10}$ and $5d^{10}$ electrons, respectively.

The electronic wavefunctions are expanded in planewaves basis sets with kinetic energy cutoffs of 70 Ry (Sb_2Se_3 , Bi_2Se_3) and 90 Ry (Sb_2S_3 , Bi_2S_3) for the calculations without semicore states, and 100 Ry (Bi_2S_3 , Bi_2Se_3) and 130 Ry (Sb_2S_3 , Sb_2Se_3) when semicore states are included. In each case considered the selected cutoff yields a total energy converged to within 2 meV/atom. All self-consistent calculations are carried out using a $8 \times 8 \times 8$ Brillouin zone mesh centered at Γ , corresponding to 170 irreducible points.

B. Crystal structure

Stibnite (Sb_2S_3), antimonelite (Sb_2Se_3), bismuthinite (Bi_2S_3), and guanajuatite (Bi_2Se_3) all crystallize in the same orthorhombic lattice and belong to the Pnma 62 space group.³⁶ Each unit cell contains 20 atoms, whose coordinates can be generated by applying the symmetry operations of the crystallographic group to a set of 5 atomic coordinates. Figure 1 shows a ball-and-stick representation of these A_2B_3 structures. The structural parameters were measured by Refs.27,50-52 and are reported in Ref. 36.

C. Quasiparticle calculations

We calculate the quasiparticle energies within many-body perturbation theory using the GW method,^{44,53–56} as implemented in the **SaX** code.⁵⁷ The GW self-energy is evaluated in the G_0W_0 approximation as $\Sigma = iG_0W_0$. Here G_0 denotes the electron Green’s function defined by the Kohn-Sham eigenstates $\psi_{n\mathbf{k}}(\mathbf{r})$ and eigenvalues $\epsilon_{n\mathbf{k}}$ corresponding to the band index n and the wavevector \mathbf{k} , and W_0 represents the screened Coulomb interaction calculated in the random phase approximation.^{53,58} The quasiparticle energies $E_{n\mathbf{k}}$ are obtained as:⁵³

$$E_{n\mathbf{k}} = \epsilon_{n\mathbf{k}} + Z_{n\mathbf{k}} \langle \psi_{n\mathbf{k}} | \Sigma(\epsilon_{n\mathbf{k}}) - V_{xc} | \psi_{n\mathbf{k}} \rangle, \quad (1)$$

where $E_{n\mathbf{k}}$ is the quasiparticle energy, $Z_{n\mathbf{k}}$ the associated quasiparticle renormalization, and V_{xc} is the exchange and correlation potential.

The self-energy can be written as the sum of a bare exchange contribution Σ_x and a correlation contribution Σ_c : $\Sigma = \Sigma_x + \Sigma_c$. The exchange part does not depend explicitly on the excitation energy and reads:⁵⁹

$$\Sigma_x(\mathbf{r}, \mathbf{r}') = - \sum_{n \in \text{occ}, \mathbf{k}} \psi_{n\mathbf{k}}^*(\mathbf{r}) \psi_{n\mathbf{k}}(\mathbf{r}') v(\mathbf{r}, \mathbf{r}'), \quad (2)$$

where the sum is over occupied states and v represents the bare Coulomb interaction. This contribution to the quasiparticle correction is sensitive to the overlap between Kohn-Sham wavefunctions regardless of their energy. As a result the use of semicore states can have significant effect on the calculations, as shown in Refs. 60–62. This aspect will be discussed in detail in Sec. III C. The energy-dependence of the correlation contribution Σ_c arising from the dynamically-screened Coulomb interaction is described via the Godby-Needs plasmon-pole model.⁶³ We use a plasmon-pole energy of 1 Ry for all materials, similar to the energy of the peaks in the calculated electron energy loss spectra.

Since the computational efforts for achieving convergence in Σ_c and Σ_x are very different owing to the necessity of evaluating unoccupied states for Σ_c , we perform separate convergence tests for these two components. For the exchange contribution we use kinetic energy cutoffs of 75 Ry and 100 Ry for calculations without and with semicore electrons, respectively. For the correlation contribution we perform convergence tests by calculating the band gap at various kinetic energy cutoffs up to 7 Ry for the polarizability. Figure 2(a) shows that the band gap is converged within 0.05 eV already for a cutoff of 5 Ry. The dependence of the band gap on the polarizability cutoff shows the same trend for calculations with or without semicore states. This is consistent with the expectation that the effect of semicore states in Σ_c should be small.⁶⁰ Based on the data of Fig. 2(a), in the following we use a polarizability cutoff of 7 Ry for calculations without semicore electrons, and of 6 Ry for the more demanding calculations including semicore states. In Fig. 2(b) we show the convergence of the band gap of

antimonelite with respect to the energy of the highest unoccupied state included in the polarizability. Based on the trend in this figure we set the number of unoccupied states to 224 and 264 for calculations with and without semicore, corresponding to a maximum energy denominator of 35 eV. Both G_0 and W_0 are calculated on uniform and Γ -centered $2 \times 6 \times 2$ Brillouin-zone meshes.

In order to estimate the accuracy of our quasiparticle corrections with respect to the above convergence parameters we follow the approach of Ref. 64. In this approach the dependence of the band gap on a given convergence parameter is fitted by a simple function in order to extract a “best-guess” asymptotic limit. This asymptotic limit is then taken to represent the converged gap. In this work we tentatively approximate gap vs. cutoff curves using the following function:

$$E_{\text{gap}}^{\text{QP}} = a_0 + a_1(x - a_2)^{-1/a_3}, \quad (3)$$

where $E_{\text{gap}}^{\text{QP}}$ is the quasiparticle band gap, x is the convergence parameter (i.e. the polarizability cutoff or the largest energy denominator) and a_0, \dots, a_3 are fitting parameters. While Eq. (3) is largely arbitrary, this choice reflects the expectation that the gap will converge faster than $1/x$ owing to the damping introduced by the matrix elements in the Adler-Wiser polarizability.^{65,66} Figure 2 shows that the fitting curves obtained for stibnite describe rather accurately the calculated data points, therefore it is reasonable to assume that the parameter a_0 obtained from the fit should provide a good estimate of the converged gap. By repeating this procedure for all four compounds Sb_2S_3 , Sb_2Se_3 , Bi_2S_3 , and Bi_2Se_3 we find that the convergence parameters described above yield band gaps which differ by less than 0.05 eV from the corresponding asymptotic values.

III. RESULTS

A. Structural parameters

Table I shows the comparison between our calculated lattice parameters and experiment. As expected the use of the local density approximation leads to a general underestimation of the experimental parameters. Interestingly, while such underestimation does not exceed 1.1% along the direction of the $(\text{A}_4\text{B}_6)_n$ ribbons (b parameter in Table I, cf. Fig. 1), the deviation can reach up to 4.2% in the direction perpendicular to the ribbons (a and c parameters in Table I). We tentatively assign this behavior to the fact that inter-ribbon forces are likely to include non-negligible van der Waals components, and hence are not described correctly within the LDA. Inspection of the calculated cohesive energies seems to support this possibility. In fact, while we calculate an intra-ribbon cohesive energy of 4.1–4.8 eV/atom for the four compounds considered, the inter-ribbon cohesive energy is only of 0.2–0.3 eV/atom.

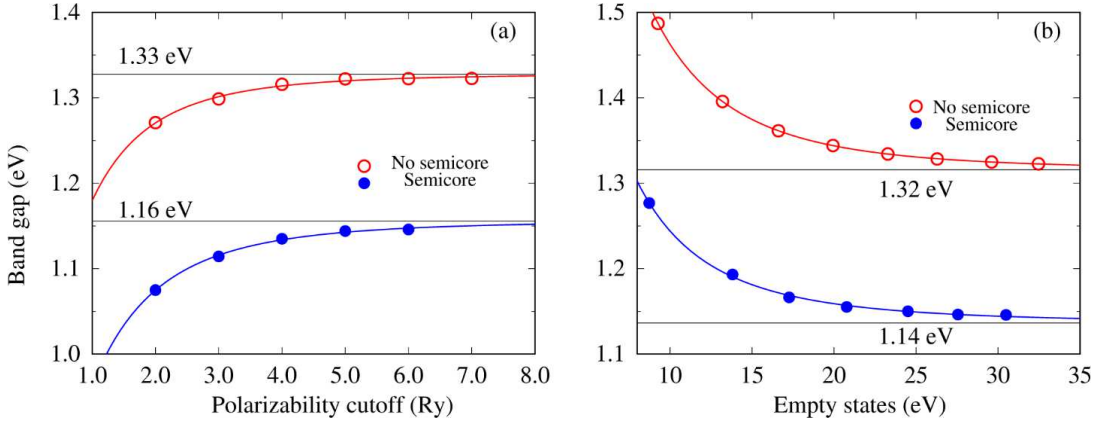


FIG. 2: (color online) Convergence tests for the quasiparticle band gap of antimonelite. (a) Calculated G_0W_0 band gap as a function of the polarizability cutoff, for calculations without (red circles) or with (blue disks) semicore states. The solid lines correspond to the fits obtained from Eq. (3). We find $a_0=1.33$ eV and 1.16 eV for calculations without and with semicore electrons, respectively. (b) Same as in (a), with the band gap reported as a function of the largest energy denominator used for calculating the polarizability. In this case we find $a_0=1.32/1.14$ eV for calculations without/with semicore electrons. All calculations were performed using optimized lattice parameters.

In order to take into account these differences between calculated and experimental lattice parameters, in the following we report quasiparticle calculations obtained for both sets of parameters.

B. DFT/LDA band structures

Figure 3 shows the DFT/LDA band structures calculated using experimental lattice parameters and without semicore electrons. Calculations including the semicore states yield very similar band structures. For clarity we only show the dispersions along the $Z-\Gamma-X$ path and along the $Y-\Gamma$ segment running along the axis of the $(A_4B_6)_n$ ribbons. The top of the valence band is found to be predominantly of S-3p or Se-4p character, while the bottom of the conduction band comprises of Sb-5p or Bi-6p states, consistently with previous calculations.^{36,42}

The band structures shown in Fig. 3 exhibit several extrema in proximity of the fundamental gap, making the direct and indirect transitions almost degenerate. Table II shows that the energy separation between direct and indirect DFT/LDA band gaps falls within 0.15 eV in all cases. The data in the table suggest that in these compounds the direct transition will most likely dominate over the indirect one, apart from a very narrow onset of 0.1-0.2 eV. This observation is consistent with experimental evidence showing a weak absorption onset just below the threshold for direct absorption.^{11,30} Therefore for practical purposes, and in particular for photovoltaics applications, stibnite, antimonelite, bismuthinite and guanajuatite can be considered as “effectively direct gap” semiconductors.

C. Quasiparticle corrections

Figure 3 shows that GW quasiparticle corrections lead to a moderate increase of the band gaps in all cases, while generally preserving the shape of the band extrema. From this figure we deduce that a simple scissor operator should be able to capture the most important effects of the GW corrections.

A detailed analysis of the quasiparticle corrections at the high-symmetry points Γ , X , and Z is given in Fig. 4 and Table III. In Fig. 4 we report the quasiparticle corrections as a function of the corresponding Kohn-Sham eigenvalues around the band extrema. In the cases of stibnite and antimonelite we observe that in the calculations with semicore electrons the valence bands are slightly upshifted (by about 0.1 eV) as compared to calculations without semicore, while the corrections to the conduction bands are essentially the same. In the cases of bismuthinite and guanajuatite the effect of semicore is to shift the valence bands up and the conduction bands down by a similar amount (~ 0.1 eV). As a result of these small changes, the quasiparticle corrections to the band gaps calculated with or without semicore electrons can differ by up to 0.2 eV (cf. Table III).

Semicore electrons appear to slightly reduce the quasiparticle corrections as compared to calculations without the semicore. This finding is consistent with previous calculations and can be rationalized as follows.⁶⁰⁻⁶² The semicore d states introduce additional contributions Σ_x^{SC} and Σ_c^{SC} to the GW self energy. Of these contributions, while the correlation part Σ_c^{SC} is small owing to the large energy separation between semicore states and conduction states, the exchange part Σ_x^{SC} can be large since it does not contain energy denominators but is sensitive to the overlap between the band edge states and the semicore states. This interpretation is confirmed by Fig. 5,

	Experiment			Calc. w/o semicore			Calc. with semicore		
	<i>a</i>	<i>b</i>	<i>c</i>	<i>a</i>	<i>b</i>	<i>c</i>	<i>a</i>	<i>b</i>	<i>c</i>
Sb ₂ S ₃	11.311 ^a	3.836 ^a	11.229 ^a	11.036 -2.4%	3.795 -1.1%	10.753 -4.2%	11.087 -2.0%	3.838 0.1%	10.834 -3.5%
Sb ₂ Se ₃	11.794 ^b	3.986 ^b	11.648 ^b	11.609 -1.6%	3.952 -0.9%	11.213 -3.7%	11.646 -1.3%	3.989 0.1%	11.287 -3.1%
Bi ₂ S ₃	11.305 ^c	3.981 ^c	11.147 ^c	11.227 -0.7%	3.999 0.5%	11.001 -1.3%	11.030 -2.4%	3.949 -0.8%	10.853 -2.6%
Bi ₂ Se ₃	11.830 ^d	4.090 ^d	11.620 ^d	11.767 -0.5%	4.141 1.3%	11.491 -1.1%	11.609 -1.9%	4.099 0.2%	11.374 -2.1%

^a Ref. 50.^b Ref. 51.^c Ref. 52.^d Ref. 27.

TABLE I: Comparison between the calculated DFT/LDA lattice parameters of stibnite, antimonelite, bismuthinite, and guanajuatite and experiment (all values are given in Å). The percentile deviation from experiment is indicated in each case.

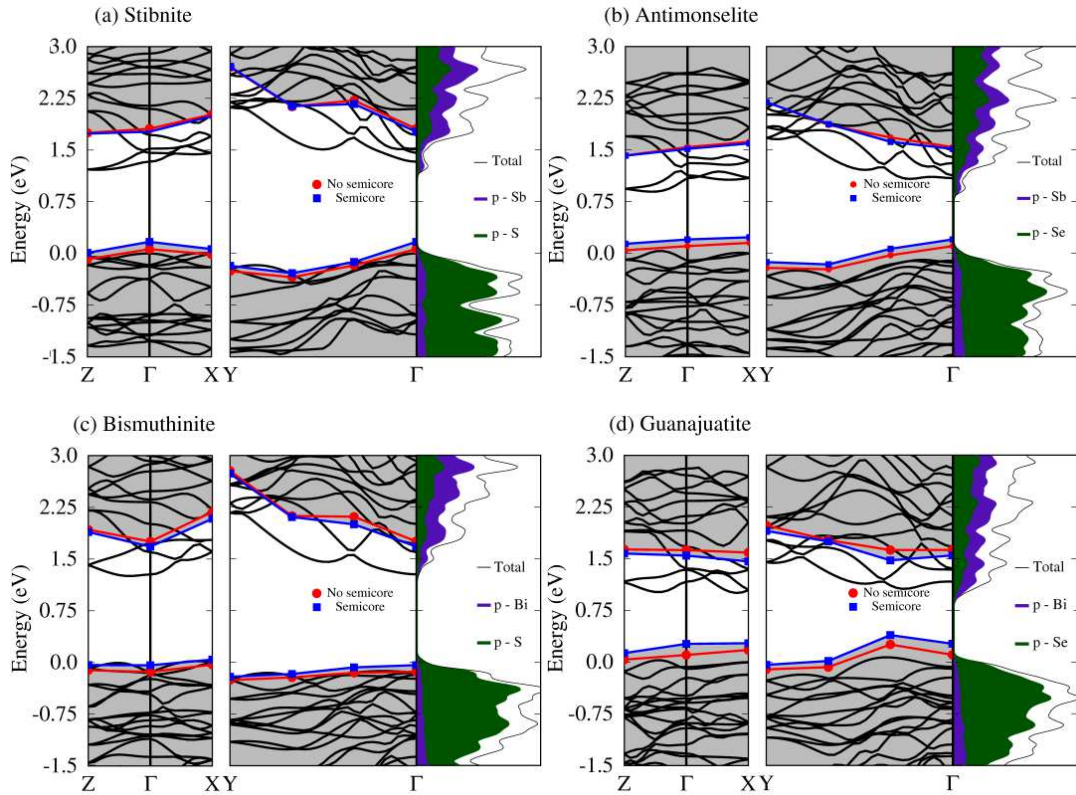


FIG. 3: (color online) Band structures of (a) stibnite, (b) antimonelite, (c) bismuthinite, and (d) guanajuatite calculated using DFT/LDA, experimental lattice parameters, and without semicore electrons (black solid lines), as well as corresponding density of states (DOS, black dashed lines). The contributions to the DOS from the *p* states of S and Se (Sb and Bi) are indicated by the green (blue) shaded areas in each case. The GW quasiparticle energies of the band extrema at high symmetry points are also shown, with blue squares and red circles indicating calculations with or without semicore electrons, respectively. The connecting lines are guides to the eye. The coordinates of the high symmetry points in reciprocal lattice units are as follows: *Z* : (0, 0, 0.5), *X* : (0.5, 0, 0), *Y* : (0, 0.5, 0).

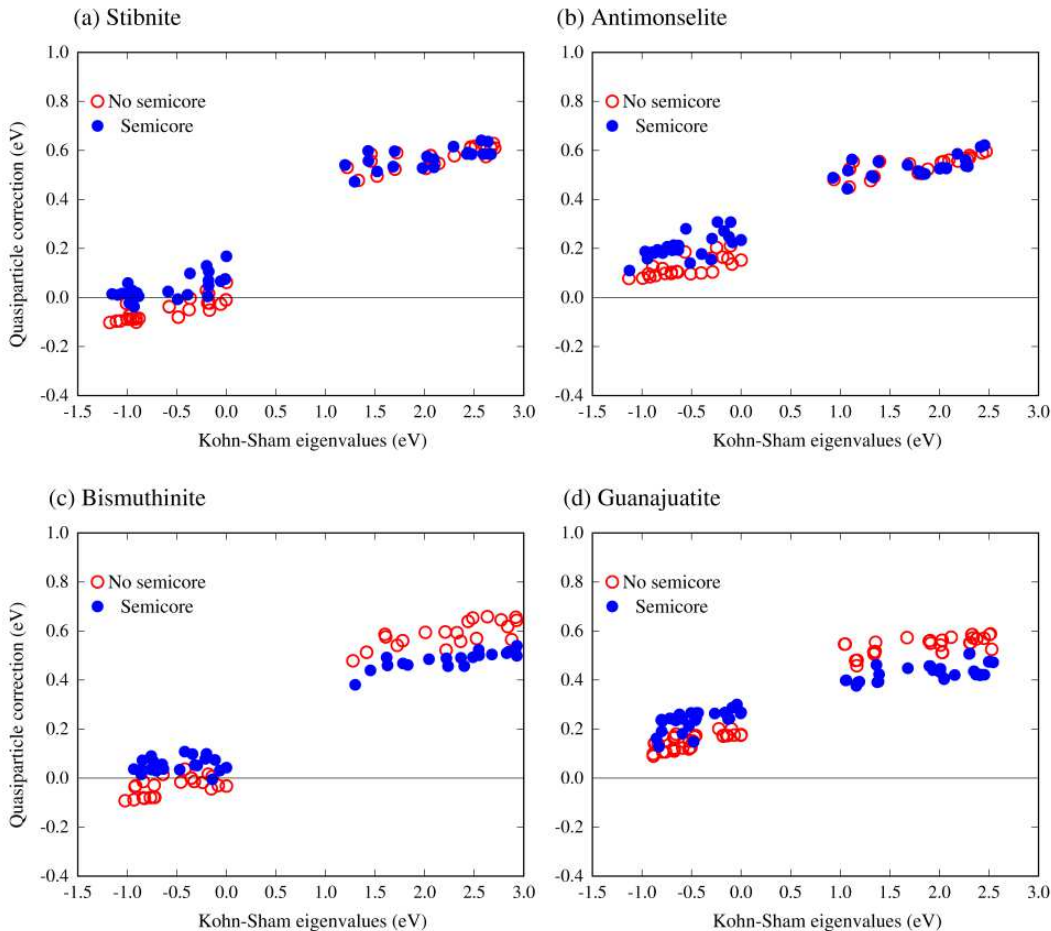


FIG. 4: Quasiparticle corrections as a function of the corresponding DFT/LDA eigenvalues for (a) stibnite, (b) antimonelite, (c) bismuthinite, and (d) guanajuatite. Only eigenvalues at the high-symmetry points Γ , X and Z are considered. Blue disks and red circles indicate calculations with and without semicore electrons, respectively.

	Minimum gap		Direct gap	
	w semicore	w/o semicore	w semicore	w/o semicore
Sb_2S_3	1.19	1.21	1.26	1.27
Sb_3Se_3	0.84	0.86	0.84	0.86
Bi_2S_3	1.25	1.24	1.28	1.27
Bi_2Se_3	0.85	0.86	0.99	0.99

TABLE II: Comparison between the minimum band gaps and the direct band gaps of stibnite, antimonelite, bismuthinite, and guanajuatite, as obtained from DFT/LDA. In these calculations we use the experimental lattice parameters. All values are in units of eV.

where we can see that the inclusion of semicore electrons does indeed affect the exchange part of the GW corrections, while at the same time the correlation component remains almost unchanged.

Generally GW quasiparticle corrections result in nega-

tive shifts of the valence band DFT/LDA eigenvalues.⁵³ At variance with this expectation in the systems considered here we find that the corrections to the valence are mostly positive (cf. Fig. 4). Cross-checking our results in a different computational framework yields the same trend.⁷⁴ This unusual trend can be linked with the remarks made for CdS in Ref. 60. In that work the authors compared the GW quasiparticle energies of CdS obtained for calculations using Cd pseudopotentials including a progressively higher number of semicore states. Their tests showed that the separation of the $n = 4$ shell into core s and p states and semicore d states led to significant inaccuracies in the exchange part of the self-energy corrections, resulting in unusual upshifts of the Cd-4d states. This problem was resolved by including the entire $n = 4$ shell in the semicore. In the present work we only include the d states of the $n = 4$ shell of Sb and the $n = 5$ shell of Bi, therefore a small systematic inaccuracy in the absolute value of the quasiparticle shifts cannot be excluded. We note however that in our case the states near the band edges are of p -character,

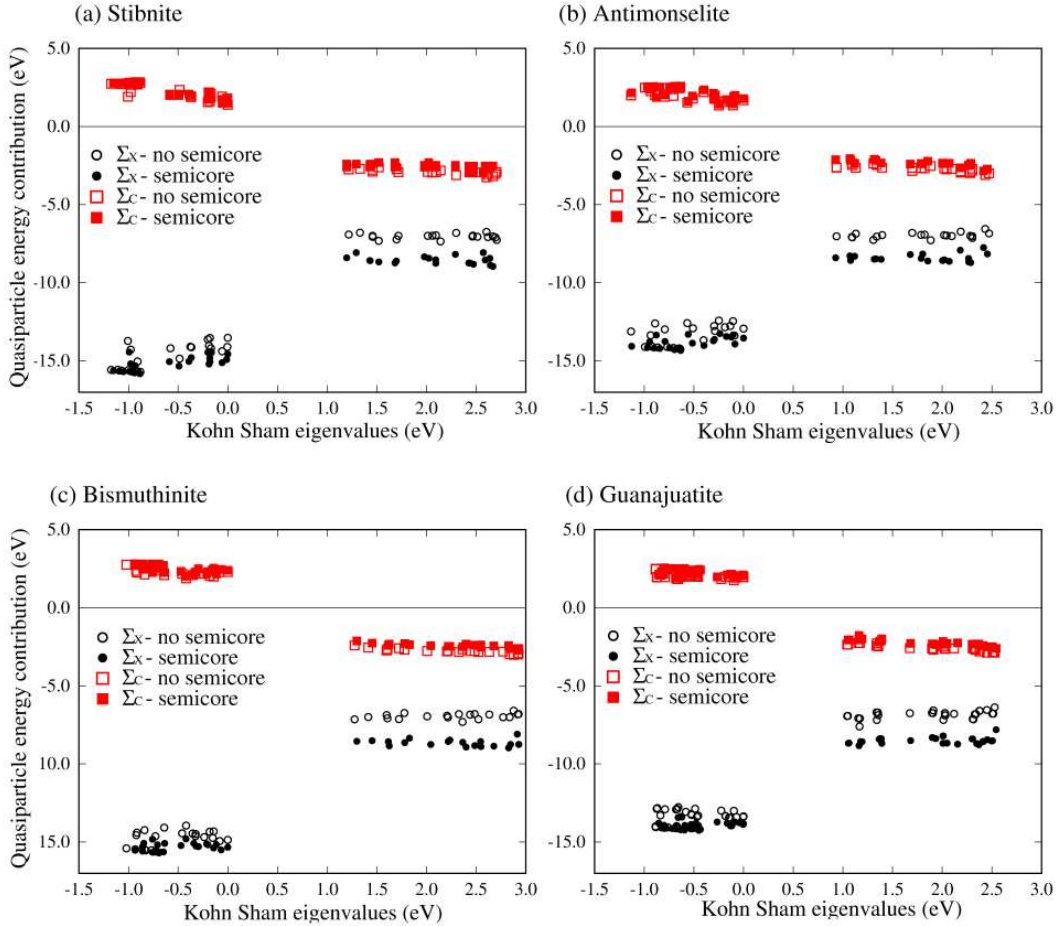


FIG. 5: Exchange (black disks and circles) and correlation (red filled and empty squares) contributions to the quasiparticle corrections vs. DFT/LDA eigenvalues for (a) stibnite, (b) antimonelite, (c) bismuthinite, and (d) guanajuatite. Only eigenvalues at the high-symmetry points Γ , X and Z are considered. Filled and empty symbols indicate calculations with and without semicore states, respectively.

therefore they should be less sensitive to the mechanism identified in Ref. 60 for the valence d states of Cd. We also point out that our calculations do not include the semicore states of Se, and this may also contribute to the upshift. Owing to the large number of atoms (20) in the unit cells of these compounds, testing these speculations would be highly impractical.

Table III reports the DFT/LDA eigenvalues and the corresponding quasiparticle corrections for the valence band top and conduction band bottom at the high symmetry points Γ , X and Z . From this table we see that the LDA band gaps at these points are sensitive to the choice of the lattice parameters, and this sensitivity is reflected in the corresponding quasiparticle energies. Calculations performed using optimized lattice parameters or experimental parameters can differ by up to 0.2 eV. This observation may explain the lack of consensus between previous computational investigations of the band structures of these compounds.^{8,36,39,43}

Taken together the sensitivity of the quasiparticle energies to the presence of semicore electrons and to the

choice of lattice parameters leads to differences in the calculated values which can be as large as 0.4 eV. This finding suggests that it is important to use extreme care when comparing the quasiparticle band structures of stibnite and related compounds with experimental data.

In the remainder of this manuscript we will focus on calculations using experimental lattice parameters and including semicore electrons, which we consider our best estimates for the quasiparticle energies in these compounds.

D. Band gaps

Table IV reports the band gaps calculated using the experimental lattice parameters and including semicore electrons. The band gaps are obtained by considering the band extrema at Γ , X , and Z , and we give both the fundamental gap and the direct gap. While in stibnite, antimonelite, and bismuthinite the calculated minimum

GW gap is indirect, the difference between direct and indirect gaps is within 0.1 eV. In guanajuatite the fundamental GW gap is direct. These results suggest that all four compounds can be considered direct-gap semiconductors for practical applications, especially in the area of optoelectronics. The calculated direct gaps are 1.60 eV (stibnite), 1.28 eV (antimonselite), 1.72 eV (bismuthinite), and 1.18 eV (guanajuatite). As shown in Table IV these values are in line with previous GW calculations where available,^{37,43} and also rather close to measured optical gaps.

The comparison with experimental data is not straightforward since the experimental literature appears to only report optical gaps (cf. literature review in Table IV). However our calculations refer to quasiparticle gaps and do not include excitonic effects. Including excitonic effects using the Bethe-Salpeter approach⁵⁶ would be rather challenging owing to the large size of these systems. To the best of our knowledge no excitonic effects were measured or mentioned for any of the four compounds studied. One exception is possibly the absorption spectrum reported in Ref. 11, which exhibits some sharp features resembling excitonic peaks, however the authors assigned those peaks to defects or internal reflections. The agreement between our calculated quasiparticle gaps and the measured optical gaps can be seen *a posteriori* as an indication that excitonic shifts are small in this class of semiconductors.

Figure 6 provides a schematic view of our calculated quasiparticle band gaps, and shows a comparison with DFT/LDA calculations and experiment.

IV. DISCUSSION

Taking the calculated quasiparticle band gaps of 1.2-1.7 eV as representative of the optical gaps, the four semiconductors considered here lie precisely in the range of the optimal Shockley-Queisser performance.⁶⁹ The Shockley-Queisser analysis addresses the ultimate efficiency of a solar cell based on a single material as light absorber and electron conductor, e.g. silicon solar cells. In this analysis the optimum efficiency results from a trade-off between maximizing the band gap in order to increase the photovoltage, and minimizing the band gap in order to increase the photocurrent.⁶⁹

In the case of nanostructured solar cells based on the donor/acceptor concept such as for instance semiconductor-sensitized solar cells,^{1,7} the Shockley-Queisser analysis needs to be modified in order to take into account the energy-level alignment at the donor/acceptor interface. In fact, while the photocurrent is still determined by the optical gap of the absorber (typically the donor), at variance with conventional bulk solar cells the photovoltage is dictated by the difference between the lowest unoccupied states of the acceptor and the highest occupied states of the donor. This effect can be taken into account by introducing the

	Optimized parameters				Expt. parameters			
	LDA		GW		LDA		GW	
	w/o S	S	w/o S	S	w/o S	S	w/o S	S
Stibnite								
Γ_v	0.00	0.00	0.10	0.20	0.00	0.00	0.06	0.17
Γ_c	1.15	1.11	1.58	1.52	1.33	1.29	1.81	1.77
X_v	-0.05	-0.03	-0.03	0.09	0.00	-0.01	-0.02	0.06
X_c	1.40	1.39	1.90	1.88	1.46	1.43	2.01	1.99
Z_v	-0.16	-0.14	-0.14	-0.04	-0.06	-0.06	-0.08	0.01
Z_c	1.17	1.17	1.65	1.65	1.22	1.20	1.75	1.74
Antimonselite								
Γ_v	-0.12	-0.12	0.07	0.18	-0.11	-0.11	0.11	0.20
Γ_c	0.97	0.91	1.40	1.32	1.09	1.07	1.54	1.52
X_v	0.00	0.00	0.19	0.29	0.00	0.00	0.15	0.23
X_c	1.05	1.00	1.53	1.46	1.10	1.08	1.62	1.60
Z_v	-0.23	-0.24	-0.06	0.02	-0.09	-0.09	0.04	0.14
Z_c	0.92	0.91	1.37	1.35	0.94	0.93	1.42	1.42
Bismuthinite								
Γ_v	-0.10	-0.04	-0.04	0.08	-0.14	-0.12	-0.14	-0.04
Γ_c	1.14	1.14	1.57	1.48	1.28	1.30	1.76	1.68
X_v	0.00	0.00	0.02	0.09	0.00	0.00	-0.03	0.04
X_c	1.50	1.67	2.04	2.09	1.61	1.63	2.18	2.09
Z_v	-0.15	-0.11	-0.13	-0.04	-0.08	-0.07	-0.11	-0.04
Z_c	1.43	1.51	1.89	1.93	1.41	1.45	1.93	1.89
Guanajuatite								
Γ_v	-0.02	-0.02	0.18	0.30	-0.07	-0.04	0.11	0.26
Γ_c	0.95	0.89	1.39	1.24	1.17	1.16	1.63	1.54
X_v	0.00	0.00	0.19	0.28	0.00	0.00	0.18	0.27
X_c	1.07	1.18	1.61	1.58	1.04	1.06	1.59	1.45
Z_v	-0.24	-0.19	-0.06	0.05	-0.14	-0.12	0.04	0.12
Z_c	1.17	1.25	1.63	1.65	1.16	1.18	1.64	1.57

TABLE III: Quasiparticle energies of stibnite, antimonselite, bismuthinite and guanajuatite at the high-symmetry points Γ , X , Z vs. the corresponding DFT/LDA eigenvalues. We report both sets of results obtained using optimized or experimental lattice parameters. The columns labelled “S” and “w/o S” indicate calculations with and without semicore electrons, respectively. For each high-symmetry point we consider the energies at the valence band top (e.g. Γ_v) and the conduction band bottom (e.g. Γ_c). All values are in units of eV.

concept of “loss-in-potential”,⁷⁰ which is the reduction of the photovoltage resulting from the energy mismatch and additional losses. Loss-in-potentials estimated for actual devices can be as large as ~ 1 eV, and the most optimistic scenario would correspond to losses as small as 0.3 eV.⁷⁰ Figure 7 shows the theoretical efficiency of semiconductor-sensitized solar cells based on stibnite, an-

	DFT		GW		Experiment
	Previous	Present	Previous	Present	
iSb ₂ S ₃	1.55 ^a , 1.76 ^b , 1.3 ^c , 1.18 ^d , 1.22 ^e	1.29 (1.20)	1.67 ^e	1.60 (1.57)	1.73 ^f , 1.42-1.65 ^g , 1.78 ^h , 1.7 ⁱ , 1.74 ^j
Sb ₂ Se ₃	1.14 ^a , 0.99 ^d , 0.79 ^k , 0.89 ^e	1.02 (0.93)	1.21 ^k	1.28 (1.19)	1.55 ^l , 1.2 ⁱ , 1.0 - 1.2 ^m
Bi ₂ S ₃	1.47 ^a , 1.32 ⁿ , 1.63 ⁿ , 1.45 ⁿ , 1.67 ⁿ	1.42 (1.30)		1.72 (1.64)	1.4 ^o , 1.38 ^p , 1.58 ^{q,j}
Bi ₂ Se ₃	0.9 ^a , 1.1 ^r	1.06		1.18	

^a Ref. 36, ^b Ref. 42, ^c Ref. 8, ^d Ref. 39, ^e Ref. 43, ^f Ref. 11,

^g Ref. 29, ^h Ref. 30, ⁱ Ref. 67, ^j Ref. 35, ^k Ref. 37, ^l Ref. 31, ^m Ref. 32,

ⁿ Ref. 41, ^o Ref. 68, ^p Ref. 33, ^q Ref. 34, ^r Ref. 40

TABLE IV: Comparison between calculated and measured band gaps of stibnite, antimonelite, bismuthinite, and guanajuatite. We report the direct band gaps calculated within DFT (Kohn-Sham gaps) and GW (quasiparticle gaps), and the measured optical gaps. The values in parenthesis indicate the calculated indirect band gaps in each case. All band gaps are in eV. The direct gaps are reported for Γ (Sb₂S₃ and Bi₂S₃), X (Bi₂Se₃), and Z (Sb₂Se₃). Our calculations include semicore electrons and were performed using the experimental lattice parameters.

timonelite, bismuthinite, and guanajuatite, calculated using the prescription of Ref. 70 for a loss-in-potential of 0.3 eV. While these estimates are very crude and the projections are possibly too optimistic, it is interesting to note that all of these four materials cluster very near the optimum power conversion efficiency of 20-25%.

From Fig. 7 we infer that the four compounds studied here are all promising candidate for nanostructured photovoltaic applications, with antimonelite and guanajuatite slightly superior to stibnite. In particular it cannot be excluded that guanajuatite, even if unstable at room temperature in bulk form, could be stabilized as a nanostructure. Given its projected maximum efficiency in Fig. 7, it might be worth to attempt the synthesis of guanajuatite nanoparticles. In the case of bismuthinite Refs. 8,9 showed that this material does not work as a semiconductor sensitizer for TiO₂, owing to the incorrect energy-level alignment at the interface. However it cannot be excluded that bismuthinite could still reach the ideal efficiency when combined with an alternative acceptor, e.g. SnO₂ or ZnO.

V. CONCLUSIONS

In this work we report a systematic study of the quasi-particle band structures of the four isostructural metal chalcogenides stibnite (Sb₂S₃), antimonelite (Sb₂Se₃), bismuthinite (Bi₂S₃), and guanajuatite (Bi₂Se₃), within the GW approximation.

In order to ensure reproducibility of our results we have placed an emphasis on convergence tests and explored the effects of various calculation parameters, such as for instance the role of semicore d electrons and lattice parameters. The inclusion of semicore electrons in the calculations is found to modify the band gaps by up to 0.2 eV, and the choice of experimental vs. optimized lattice parameters can lead to differences of up to 0.2 eV in the calculated gaps. These findings indicate that some caution should be used in discussing the theoretical band gaps of

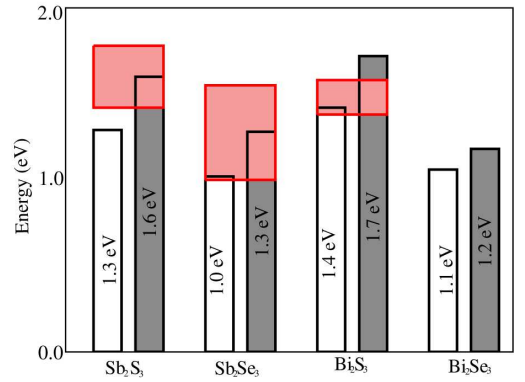


FIG. 6: Schematic summary of the band gaps of stibnite, antimonelite, bismuthinite, and guanajuatite calculated in this work: Kohn-Sham gaps (empty rectangles) and GW gaps (filled rectangles). The band gaps were obtained by including semicore electrons and using the experimental lattice parameters. The pink rectangles indicate the range of experimental optical gaps reported in Table IV

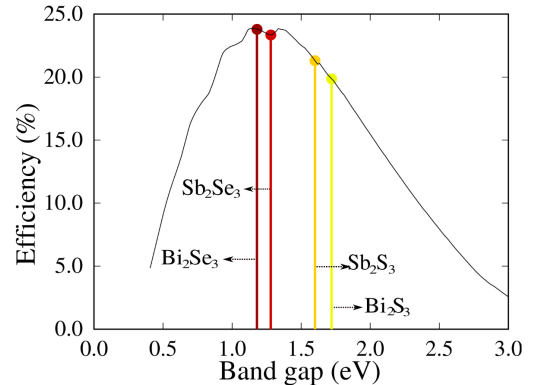


FIG. 7: Ideal efficiency of nanostructured solar cells based on semiconductors of the stibnite family. The theoretical efficiency as a function of the band gap energy (black solid curve) is calculated using the prescription of Ref. 70 with a loss-in-potential of 0.3 eV and a fill factor of 73%.

these materials and in comparing with experiment.

Our calculations indicate that all four compounds have direct band gaps, barring indirect transitions marginally below the direct gap. The calculated band gaps are 1.6 eV (stibnite), 1.3 eV (antimonelite), 1.7 eV (bismuthinite) and 1.2 eV (guanajuatite). These values fall within the range of measured optical gaps, although it must be observed that there is a considerable scatter in the experimental data, possibly due to different preparation conditions.

Using a modified Shockley-Queisser analysis,⁷⁰ we estimate the ultimate performance of solar cells based on these compounds as light sensitizers. This analysis indicates that all four materials have potential for high-efficiency nanostructured solar cells. The highest theoretical efficiency is obtained for guanajuatite, the high-temperature polymorph of the topological insulator Bi_2Se_3 . This finding suggests that it could be worth attempting to synthesize nanoparticles of this compound (which is unstable in bulk form at room temperature). Future calculations should address the optical absorption

spectra of these compounds within the Bethe-Salpeter approach, in order to establish whether excitonic effects are small as our data appear to suggest. It will be also interesting to extend the present study to the case of individual nanoribbons of these metal chalcogenides, since liquid-phase exfoliation techniques for van der Waals bonded materials are becoming increasingly popular.⁷¹

We hope that the present study will contribute to the ongoing research on new materials for energy applications, and stimulate further efforts to understand and exploit these fascinating and relatively unexplored compounds.

Acknowledgments

This work is supported by the UK EPSRC and the ERC under EU FP7/ERC Grant No. 239578. Calculations were performed at the Oxford Supercomputing Centre. Figures rendered using Xcrysden.⁷²

- ¹ J. A. Chang, J. H. Rhee, S. H. Im, Y. H. Lee, H. Kim, S. I. Seok, M. K. Nazeeruddin, and M. Grätzel, *Nano Lett.* **10**, 2609 (2010).
- ² J. A. Chang, S. H. Im, Y. H. Lee, H. Kim, C.-S. Lim, J. H. Heo, and S. I. Seok, *Nano Lett.* **12**, 1863 (2012).
- ³ A. K. Rath, M. Bernechea, L. Martinez, F. P. Garcia de Arquer, J. Osmond, and G. Kostantatos, *Nature Photonics* **6**, 529 (2012).
- ⁴ N. Guijarro, T. Lutz, T. Lana-Villarreal, F. O'Mahony, R. Gomez, and S. A. Haque, *J. Phys. Chem. Lett.* **3**, 1351 (2012).
- ⁵ R. J. Mehta, C. Karthik, W. Jiang, B. Singh, Y. Shi, R. Siegel, T. Borca-Tasciuc, and G. Ramanath, *Nano. Lett.* **10**, 4417 (2010).
- ⁶ B. O'Regan and M. Grätzel, *Nature* **353**, 737 (1991).
- ⁷ G. Hodes, *J. Phys. Chem. C* **112**, 17778 (2008).
- ⁸ C. E. Patrick and F. Giustino, *Adv. Funct. Mater.* **21**, 4663 (2011).
- ⁹ T. Lutz, A. MacLachlan, A. Sudlow, J. Nelson, M. S. Hill, K. C. Molloy, and S. A. Haque, *Phys. Chem. Chem. Phys.* **14**, 16192 (2012).
- ¹⁰ C. H. Bhosale, M. D. Uplane, P. S. Patil, and C. D. Lokhande, *Thin Solid Films* **248**, 137 (1994).
- ¹¹ M. Y. Versavel and J. A. Haber, *Thin Solid Films* **515**, 7171 (2007).
- ¹² C. D. Lokhande, B. R. Sankapal, R. S. Mane, H. M. Pathan, M. Muller, M. Giersig, and V. Ganesan, *Appl. Surf. Sci.* **193**, 1 (2002).
- ¹³ H. Maghraoui-Meherzi, T. Ben Nasr, N. Kamoun, and M. Dachraoui, *Physica B* **405**, 3101 (2010).
- ¹⁴ L. Cademartiri, R. Malakooti, P. G. O'Brien, S. Petrov, N. P. Kherani, and G. A. Ozin, *Angew. Chem. Int. Ed.* **47**, 3814 (2008).
- ¹⁵ R. Malakooti, L. Cademartiri, A. Migliori, and G. A. Ozin, *J. Mater. Chem* **18**, 66 (2008).
- ¹⁶ S. Rühle, M. Shalom, and A. Zaban, *Chem. Phys. Chem* **11**, 2290 (2010).
- ¹⁷ Q. Han, S. Sun, D. Sun, J. Zhu, and X. Wang, *RSC Adv.* **1**, 1364 (2011).
- ¹⁸ L. Cademartiri, G. Guerin, K. J. Bishop, and M. A. Winnik, *J. Am. Chem. Soc.* **134**, 9327 (2012).
- ¹⁹ M. E. Rincon, M. Sanchez, P. J. George, A. Sanchez, and P. K. Nair, *J. Solid State Chem.* **136**, 167 (1998).
- ²⁰ F. Perales, G. Lifante, F. Agulló-Rueda, and C. de la Heras, *J. Phys. D: Appl. Phys.* **40**, 2440 (2007).
- ²¹ H. Bao, X. Cui, C. M. Li, Q. Song, Z. Lu, and J. Guo, *J. Phys. Chem. C* **111**, 17131 (2007).
- ²² A. G. Vedeshwar, *J. Phys. III France* **5**, 1161 (1995).
- ²³ A. M. Karguppikar and A. G. Vedeshwar, *Phys. Lett. A* **126**, 123 (1987).
- ²⁴ Z. Deng, M. Mansuripur, and A. J. Muscat, *Nano. Lett.* **9**, 2015 (2009).
- ²⁵ J. Varghese, S. Barth, L. Keeney, R. W. Whatmore, and J. D. Holmes, *Nano. Lett.* **12**, 868 (2012).
- ²⁶ H. Zhang, C. X. Liu, X. L. Qi, Z. Fang, and S.-C. Zhang, *Nature Physics* **5**, 438 (2009).
- ²⁷ E. Y. Atabaeva, S. A. Mashkov, and S. V. Popova, *Sov. Phys. Crystallogr.* **18**, 173 (1973).
- ²⁸ H. Okamoto, *J. Phase. Equilib.* **15**, 195 (1994).
- ²⁹ S. Mahanty, J. M. Merino, and M. León, *J. Vac. Sci. Technol. A* **15**, 3060 (1997).
- ³⁰ I. K. El Zawawi, A. Abdel-Moez, F. S. Terra, and M. Mounir, *Thin Solid Films* **324**, 300 (1998).
- ³¹ A. P. Torane, K. Y. Rajpure, and C. H. Bhosale, *Mater. Chem. Phys.* **61**, 219 (1999).
- ³² Y. Rodriguez-Lazcano, Y. Pena, M. T. S. Nair, and P. K. Nair, *Thin Solid Films* **493**, 77 (2005).
- ³³ J. Lukose and B. Pradeep, *Sol. State. Comm.* **78**, 535 (1991).
- ³⁴ S. Mahmoud, A. H. Eid, and H. Omar, *Fizika A* **3**, 111 (1997).
- ³⁵ N. S. Yesugade, C. D. Lokhande, and C. H. Bhosale, *Thin Solid Films* **263**, 145 (1995).
- ³⁶ R. Caracas and X. Gonze, *Phys. Chem. Minerals* **32**, 295

- (2005).
- ³⁷ R. Vadapoo, S. Krishnan, H. Yilmaz, and C. Marin, *Phys. Status Solidi B* **248**, 700 (2011).
 - ³⁸ P. Larson, V. A. Greanya, W. C. Tonjes, R. Liu, S. D. Mahanti, and C. G. Olson, *Phys. Rev. B* **65**, 085108 (2002).
 - ³⁹ H. Koc, A. M. Mamedov, E. Deligoz, and H. Ozisik, *Sol. State. Sci.* **14**, 1211 (2012).
 - ⁴⁰ Y. Sharma and P. Srivastava, *AIP Conf. Proc.* **1249**, 183 (2010).
 - ⁴¹ Y. Sharma, P. Srivastava, A. Dashora, L. Vadkhiya, M. K. Bhayani, R. Jain, A. R. Jani, and B. L. Ahuja, *Sol. State Sci.* **14**, 241 (2012).
 - ⁴² T. Ben Nasr, H. Maghraoui-Meherzi, H. Ben Abdallah, and R. Bennaceur, *Physica B* **406**, 287 (2011).
 - ⁴³ R. Vadapoo, S. Krishnan, H. Yilmaz, and C. Marin, *Nanotechnology* **22**, 175705 (2011).
 - ⁴⁴ L. Hedin, *Phys. Rev.* **139**, A796 (1965).
 - ⁴⁵ P. Giannozzi et al., *J. Phys.: Condens. Matter.* **21**, 395502 (19pp) (2009).
 - ⁴⁶ J. P. Perdew and A. Zunger, *Phys. Rev. B* **23**, 5048 (1981).
 - ⁴⁷ D. M. Ceperley and B. J. Alder, *Phys. Rev. Lett.* **45**, 566 (1980).
 - ⁴⁸ N. Troullier and J. L. Martins, *Phys. Rev. B* **43**, 1993 (1991).
 - ⁴⁹ M. Fuchs and M. Scheffler, *Comp. Phys. Comm.* **119**, 67 (1999).
 - ⁵⁰ P. Bayliss and W. Nowacki, *Z Kristall* **135**, 308 (1972).
 - ⁵¹ G. P. Voutsas, A. G. Papazoglou, and P. J. Rentzeperis, *Z Kristall* **171**, 261 (1985).
 - ⁵² A. S. Kanishcheva, Y. N. Mikhailov, and A. F. Trippel, *Izv. Akad. Nauk. SSSR. Neorganicheskie Mater.* **17**, 1972 (1981).
 - ⁵³ M. S. Hybertsen and S. G. Louie, *Phys. Rev. B* **34**, 5390 (1986).
 - ⁵⁴ W. G. Aulbur, L. Jönsson, and J. W. Wilkins, *Solid State Phys.* **54**, 1 (1999).
 - ⁵⁵ F. Aryasetiawan and O. Gunnarsson, *Rep. Prog. Phys* **61**, 237 (1998).
 - ⁵⁶ G. Onida, L. Reining, and A. Rubio, *Rev. Mod. Phys* **74**, 601 (2002).
 - ⁵⁷ L. Martin-Samos and G. Bussi, *Comp. Phys. Comm.* **180**, 1416 (2009).
 - ⁵⁸ L. Hedin and S. Lundqvist, *Solid State Physics* **23**, 1 (1969).
 - ⁵⁹ F. Giustino, M. L. Cohen, and S. G. Louie, *Phys. Rev. B* **81**, 115105 (2010).
 - ⁶⁰ M. Rohlfing, P. Krüger, and J. Pollmann, *Phys. Rev. Lett.* **75**, 3489 (1995).
 - ⁶¹ M. L. Tiago, S. Ismail-Beigi, and S. G. Louie, *Phys. Rev. B* **69**, 125212 (2004).
 - ⁶² P. Umari and S. Fabris, *J. Chem. Phys* **136**, 174310 (2012).
 - ⁶³ R. W. Godby and R. J. Needs, *Phys. Rev. Lett.* **62**, 1169 (1989).
 - ⁶⁴ S. Sharifzadeh, I. Tamblyn, P. Doak, P. T. Darancet, and J. B. Neaton, *Europ. Phys. J.* **85**, 323 (2012).
 - ⁶⁵ S. L. Adler, *Phys. Rev.* **126**, 413 (1962).
 - ⁶⁶ N. Wiser, *Phys. Rev.* **129**, 62 (1963).
 - ⁶⁷ J. Black, E. N. Conwell, L. Sigle, and C. W. Spencer, *J. Phys. Chem. Solids* **2**, 240 (1957).
 - ⁶⁸ L. Gildart, J. M. Kline, and D. M. Mattox, *J. Phys. Chem. Sol.* **18**, 286 (1961).
 - ⁶⁹ W. Shockley and H. J. Queisser, *J. Appl. Phys.* **32**, 510 (1961).
 - ⁷⁰ H. J. Snaith, *Adv. Func. Mater.* **20**, 13 (2010).
 - ⁷¹ J. N. Coleman et al., *Science* **331**, 568 (2011).
 - ⁷² A. Kokalj, *Comp. Mater. Sci.* **28**, 155 (2003).
 - ⁷³ A. Marini, C. Hogan, M. Gruning, and D. Versano, *Comp. Phys. Comm.* **180**, 1392 (2009).
 - ⁷⁴ We perform identical calculations using the code *Yambo*⁷³ and obtain similar upshifts of the valence band.